Mon. Not. R. Astron. Soc. **000**, 1–14 (2010) Printed 9 December 2010 (MN LATEX style file v1.4)

Rotation speed of the first stars

Athena Stacy[1⋆], Volker Bromm[1] and Abraham Loeb[2]
[1] *Department of Astronomy and Texas Cosmology Center, University of Texas, Austin, TX 78712, USA*
[2] *Astronomy Department, Harvard University, 60 Garden Street, Cambridge, MA 02138, USA*

9 December 2010

ABSTRACT

We estimate the rotation speed of Population III (Pop III) stars within a minihalo at $z \sim 20$ using a smoothed particle hydrodynamics (SPH) simulation, beginning from cosmological initial conditions. We follow the evolution of the primordial gas up to densities of 10^{12} cm^{-3}. Representing the growing hydrostatic cores with accreting sink particles, we measure the velocities and angular momenta of all particles that fall onto these protostellar regions. This allows us to record the angular momentum of the sinks and estimate the rotational velocity of the Pop III stars expected to form within them. The rotation rate has important implications for the evolution of the star, the fate encountered at the end of its life, and the potential for triggering a gamma-ray burst (GRB). We find that there is sufficient angular momentum to yield rapidly rotating stars ($\gtrsim 1000$ km s^{-1}, or near break-up speeds). This indicates that Pop III stars likely experienced strong rotational mixing, impacting their structure and nucleosynthetic yields. A subset of them was also likely to result in hypernova explosions, and possibly GRBs.

Key words: cosmology: theory – early Universe – galaxies: formation – stars: formation.

1 INTRODUCTION

The first stars, also known as Population III (Pop III) stars, are believed to be early drivers of cosmic evolution (e.g. Barkana & Loeb 2001; Bromm & Larson 2004; Ciardi & Ferrara 2005; Glover 2005; Bromm et al. 2009; Loeb 2010). These stars are thought to have formed around $z \sim 20$ within minihaloes of mass $M \sim 10^6$ M$_\odot$ (e.g. Haiman et al. 1996; Tegmark et al. 1997; Yoshida et al. 2003). Not only did the radiation from the first stars likely start the process of reionizing the intergalactic medium (IGM; e.g. Kitayama et al. 2004; Sokasian et al. 2004; Whalen et al. 2004; Alvarez et al. 2006; Johnson et al. 2007), but when some of these stars produced supernovae (SNe) explosions, they released the first heavy elements into the IGM, providing its initial metal enrichment (e.g. Madau et al. 2001; Mori et al. 2002; Bromm et al. 2003; Wada & Venkatesan 2003; Norman et al. 2004; Tornatore et al. 2007; Greif et al. 2007, 2010; Wise & Abel 2008).

The mass of the first stars is the main factor in determining their cosmological impact. Pop III stars are generally believed to be very massive (~ 100 M$_\odot$; e.g. Abel et al. 2002; Bromm et al. 2002), though recent evidence for fragmentation in primordial gas may imply that the typical Pop III mass was somewhat lower (Clark et al. 2008, 2010; Turk et al. 2009; Stacy et al. 2010). The stellar luminosity and ionizing photon production primarily depend on mass, as does the end state of the star. For instance, stars between 40 M$_\odot$ and 140 M$_\odot$ are expected to collapse directly into black holes, while stars in the mass range of 140 M$_\odot$ $< M_* <$ 260 M$_\odot$ will die as pair-instability supernovae (PISNe; Heger & Woosley 2002). Below 40 M$_\odot$, stars are again expected to explode as core-collapse SNe, leaving behind a neutron star or black hole. Nomoto et al. (2003), however, find that the nature of the explosions from this mass range may vary depending on the angular momentum of the collapsing core. Stars with little angular momentum will explode as faint SNe, while stars of the same mass but higher angular momentum will become extremely energetic hypernovae.

Pop III stars also have the potential to produce gamma-ray bursts (GRBs), particularly given the connection between long-duration GRBs and the deaths of massive stars (see Woosley & Bloom 2006). GRBs may provide one of the most promising methods of directly probing the final stages of Pop III stars, provided they occurred with a high enough frequency (e.g. Bromm & Loeb 2002, 2006; Gou et al. 2004; Belczynski et al. 2007). Naoz & Bromberg (2007) used early *Swift* data and an idealized star formation rate model to estimate that Pop III stars may indeed produce GRBs at an efficiency of $\sim 10^{-4}$ GRBs per solar mass incorporated in primordial stars. For the collapsar model of GRB generation

⋆ E-mail: minerva@astro.as.utexas.edu

to operate, this will require sufficient angular momentum in the Pop III progenitor for an accretion torus to form around the remnant black hole (e.g. Woosley 1993; Lee & Ramirez-Ruiz 2006). The progenitor star must also lose its hydrogen envelope to enable the relativistic jet to penetrate through and exit the star (e.g. Zhang et al. 2004). Fulfilling both of these conditions can be difficult for a single-star progenitor, however, because removing the extended hydrogen envelope will also lead to removal of angular momentum in the core (e.g. Spruit 2002; Heger et al. 2005; Petrovic et al. 2005). These conditions for a GRB may be more easily met, however, in a close binary system that experiences Roche lobe overflow (e.g. Lee et al. 2002; Izzard et al. 2004). Let us also note an alternate scenario recently explored by Suwa & Ioka (2010). They analytically find that the jet can break out even from an extended hydrogen envelope of a Pop III star if the jet is powered by magnetic fields. This interesting result warrants further numerical study.

Another possibility arises if a Pop III star has a large enough spin. This can affect its nucleosynthesis and change the evolution off the main sequence (MS), opening a new pathway for the formation of single-star progenitor GRBs (e.g. Yoon & Langer 2005; Woosley & Heger 2006; Ekström et al. 2008a). Woosley & Heger (2006) find through their stellar evolution models that very massive ~ 20 M$_\odot$ stars rapidly rotating at $\simeq 400$ km s^{-1} ($\simeq 40\%$ of the break-up speed) can completely mix while on the MS, bypassing the red giant phase and becoming a Wolf-Rayet (WR) star. This evolutionary path may furthermore allow the star to retain enough angular momentum to become a GRB, particularly if the star has low-metallicity and thus experiences significantly reduced mass loss compared to solar-metallicity WR stars. Yoon & Langer (2005) agree, using a different numerical methodology, that rotationally induced mixing will allow a low-metallicity massive star to evolve into a rapidly rotating WR star and potentially a GRB. Finally, Ekström et al. (2008a) studied the evolution of metal-free stars with a range of masses (15-200 M$_\odot$) and a high rotation rate of 800 km s^{-1}, corresponding to a fraction of 40-70% of their break-up speed. In contrast to the previous studies, in their models chemical mixing was usually not sufficient for the red giant phase to be avoided. In fact, they found that the rotating stars generally end their lives at a cooler location of the Hertzsprung-Russel diagram (HRD). In addition, rotating stars produced a higher amount of metals, compared to their non-rotating counterparts. Ekström et al. (2008a) attribute this difference to the fact that, unlike the earlier studies, they did not include the magnetic dynamo mechanism of Spruit (2002). With or without this mechanism, however, all studies conclude that stellar rotation altered the evolution and fate of low-metallicity and Pop III stars. We also point out that, though we sometimes refer to low-metallicity studies, Pop III evolution is distinct from that of low-metallicity, and results for one do not simply extrapolate to the other (e.g. Ekström et al. 2008b). This highlights the need for continued investigation of rotating metal-free stars.

It is apparent that the angular momentum of Pop III stars plays a key role in their evolution and death, as well as their subsequent impact on the IGM. Whereas the mass scale of the first stars has been investigated in numerous studies, their spin remains poorly understood. It is an open question whether Pop III stars can realistically attain the high spin needed for the above-mentioned processes to occur. Current observations of massive O and B-type stars in our Galaxy and the Large Magellanic Cloud show that they can indeed be rapid rotators, spinning at a significant percentage of break-up speed (a few tens of percent). They have a large range of spin, from several tens of km s^{-1} to well over 300 km s^{-1}, with an average of about 100–200 km s^{-1} (e.g. Huang & Gies 2008; Wolff et al. 2008). This does not necessarily apply to Pop III stars, however, which formed in a different environment. While Pop III stars formed in minihaloes whose gravitational potential wells were dominated by dark matter (DM), massive stars today form within molecular clouds that are not DM dominated, and are embedded in much larger galaxies. The angular momentum in the latter case ultimately derives from galactic differential rotation on the largest scales, and turbulence in the interstellar medium (ISM) on smaller scales (see, e.g. Bodenheimer 1995). Wolff et al. (2008) argue that their measured stellar rotation rates reflect the initial conditions of the cores in which the stars formed, particularly the core turbulent speeds and resulting infall rates. To better determine the possible rotation rates of Pop III stars, it is thus necessary to study the environment specific to where they formed.

To better understand the potential for the various spin-dependent evolutionary pathways of Pop III stars, we perform a three-dimensional cosmological simulation that follows the evolution of primordial gas in a minihalo to densities of $n > 10^{12}$ cm^{-3}. Similar to Bromm & Loeb (2004) and Stacy et al. (2010), we represent gravitationally collapsing high-density peaks using the sink particle method first introduced by Bate et al. (1995). This allows us to follow the mass flow onto the sinks for many (~ 100) dynamical times. As a sink particle grows in mass, the angular momentum of the accreted mass is recorded, allowing us to measure the total angular momentum of the sink and estimate the spin of the Pop III star represented by the sink. This is very similar to the method used in Jappsen & Klessen (2004) when they studied the angular momentum evolution of protostellar cores, though their calculation had lower resolution and was designed to study modern-day star formation as seen in the ISM. We give further details concerning our numerical methodology in §2, while in §3 we present our results, including estimates of the stellar rotation rate. In §4 we discuss the implications for the evolution and death of Pop III stars, and in §5 we address the possibility of sub-sink fragmentation. We summarize our main conclusions in §6.

2 NUMERICAL METHODOLOGY

2.1 Initial Setup

Similar to the method used in Stacy et al. (2010), we carry out our study using GADGET, a three-dimensional smoothed particle hydrodynamics (SPH) code (Springel et al. 2001; Springel & Hernquist 2002). We perform the final part of the simulation described in Stacy et al. (2010) again, starting from approximately 4000 years (~ 100 free-fall times) before the first sink particle forms. This simulation was originally initialized at $z = 99$ in a periodic box of length 100 h^{-1} kpc using both SPH and DM particles.

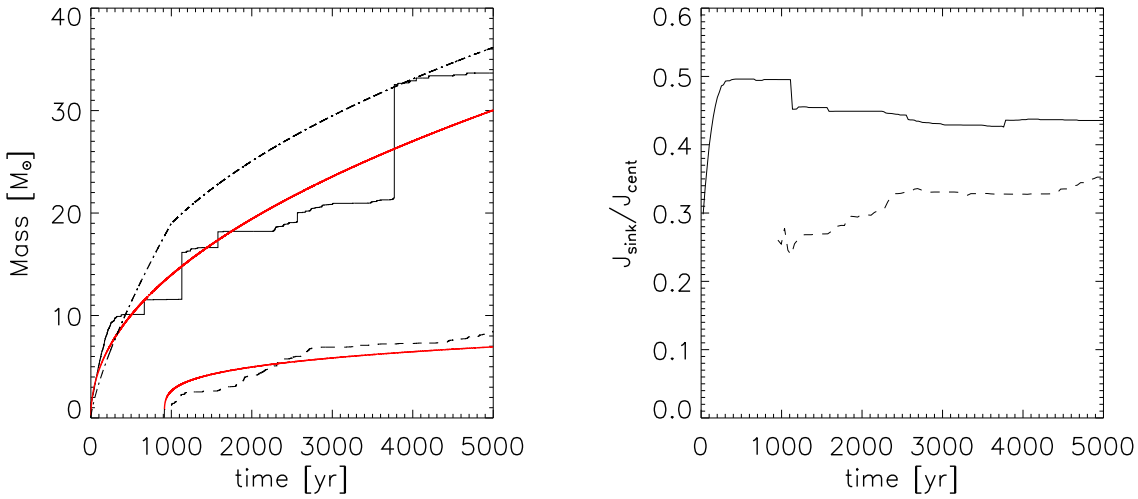

Figure 1. *Left*: Growth of sink mass over time. Solid line is the growth of sink A, and dashed line is the growth of sink B. Dash-dot line is the result from Bromm & Loeb (2004). Red lines are power-law fits to the mass curves. Though sink A grows rapidly for the first few hundred years, adding the accretion criterion of non-rotational support later causes its growth rate to be somewhat lower than that found in Bromm & Loeb (2004) until a large merger event at 3800 years. *Right*: Ratio $\epsilon = J_{\rm sink}/J_{\rm cent}$ as sinks grow over time. Representation of different sinks is the same as in the left panel. For sink B's accretion and the first ~ 1000 years of sink A's accretion, note the similarity in how both mass and ϵ increase over time. This is due to the steadily growing rotational support of the mass that flows onto the sinks.

This was done in accordance with a ΛCDM cosmology with $\Omega_\Lambda = 0.7$, $\Omega_{\rm M} = 0.3$, $\Omega_{\rm B} = 0.04$, and $h = 0.7$. To accelerate structure formation, we chose an artificially enhanced normalization of the power spectrum of $\sigma_8 = 1.4$. We have verified that the density and velocity fields in the center of the minihalo are very similar to previous simulations. Even though we used an artificially high value of σ_8, the angular momentum profile of our minihalo just before sink formation was still very similar to that of other cosmological simulations which used lower σ_8 values. In particular, the cosmological simulation of Yoshida et al. (2006), which used $\sigma_8 = 0.9$, and that of Abel et al. (2002), which used $\sigma_8 = 0.7$, resulted in minihalo profiles which were especially similar to ours on the smaller scales from which the mass of the sinks is accreted. This demonstrates that our realization leads to conditions that are typical for primordial star formation (see the discussion in Stacy et al. 2010).

To achieve high resolution we employed a standard hierarchical zoom-in procedure (see Stacy et al. 2010 for further details). This involved adding three additional nested refinement levels of length 40, 30, and 20 kpc (comoving) centered on the site where the first minihalo will form. Each level of higher refinement replaces particles from the lower level with eight child particles such that in the final simulation a parent particle is replaced by up to 512 child particles. The highest-resolution gas particles have a mass of $m_{\rm SPH} = 0.015$ M$_\odot$. Therefore, the mass resolution of the refined simulation is: $M_{\rm res} \simeq 1.5 N_{\rm neigh} m_{\rm SPH} \lesssim 1$ M$_\odot$, where $N_{\rm neigh} \simeq 32$ is the typical number of particles in the SPH smoothing kernel (e.g. Bate & Burkert 1997). The main difference between the current simulation and that described in Stacy et al. (2010) is that we now record the angular momenta and velocities of the sink-accreted particles before they become incorporated into the sinks. This allows us to track the total spin of the sink particles as they grow in mass.

2.2 Chemistry, heating, and cooling

The chemistry, heating, and cooling of the primordial gas is treated similarly to that in earlier studies such as Bromm & Loeb (2004), Yoshida et al. (2006), and Stacy et al. (2010). We track the abundance evolution of the following species: H, H^+, H^-, H_2, H_2^+, He, He^+, He^{++}, e^-, and the deuterium species D, D^+, D^-, HD, and HD^+. In the high-density disk that forms within the minihalo, H_2 is the dominant cooling agent, and although deuterium is unimportant for the thermal and chemical evolution of the gas at the late stages of collapse and accretion studied here, we include it for completeness. We use the same chemical network and the same cooling and heating terms as used in Stacy et al. (2010). This included accounting for modified physics at densities greater than $\simeq 10^8$ cm^{-3}: three-body processes which accelerate the formation of H_2 until the gas becomes fully molecular around $\simeq 10^{10}$ cm^{-3}, enhanced cooling due to collisions between H_2 molecules, H_2 formation heating, and modified values for the adiabatic exponent $\gamma_{\rm ad}$ and the mean molecular weight μ. As described in Stacy et al. (2010), the evolution of the primordial gas up to the formation of the first sink particle was consistent with that of previous studies.

2.3 Sink Particle Method

We convert an SPH particle into a sink particle if it reaches a number density of $n_{\rm max} = 10^{12}$ cm^{-3}. SPH particles that are within a distance $r_{\rm acc}$ of the sink are removed from the simulation and their mass is also added to that of the sink, provided that they are not rotationally supported against

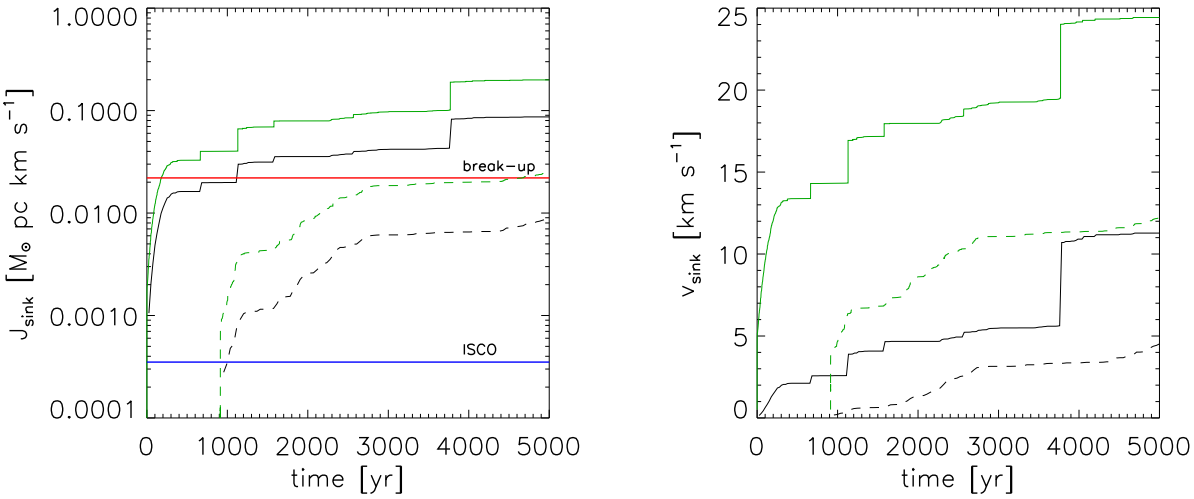

Figure 2. *Left*: Angular momentum $J_{\rm sink}$ of the sinks over time, taken by summing the angular momentum $J_{\rm SPH} = m_{\rm SPH} v_{\rm rot} d$ of each accreted particle just before it is added onto the sink. Solid black line represents sink A, dashed black line represents sink B. The angular momentum of each sink grows as it accretes more mass, always staying at a fraction of $J_{\rm cent}$ (solid green line for sink A, dashed green line for sink B). Note that for sink A, $J_{\rm sink}$ exceeds the stellar $J_{\rm break-up}$ (red line) by the end of the simulation. The horizontal blue line shows the orbital angular momentum at the *innermost stable circular orbit (ISCO)*, $J_{\rm ISCO}$, for a 100 $M_\odot$ black hole. This value is well exceeded by $J_{\rm sink}$ of both sinks. *Right*: Sink rotational velocity, $v_{\rm sink}$, measured at $r = r_{\rm acc}$ (with sink A denoted by a solid black line, and sink B by a dashed black line). Values for $v_{\rm sink}$ are recorded as the mass-weighted average of $v_{\rm rot}$ for all accreted particles. The upper (green) lines for each line type represent the velocity needed for centrifugal support, $v_{\rm cent}$. Note that $v_{\rm sink}$ stays at a nearly constant fraction of $v_{\rm cent}$.

infall towards the sink. We set $r_{\rm acc}$ equal to the resolution length of the simulation, $r_{\rm acc} = L_{\rm res} \simeq 50\,{\rm AU}$, where:

$$L_{\rm res} \simeq 0.5 \left(\frac{M_{\rm res}}{\rho_{\rm max}} \right)^{1/3},$$

with $\rho_{\rm max} \simeq n_{\rm max} m_{\rm H}$ and $m_{\rm H}$ being the proton mass. The sink particle's mass, $M_{\rm sink}$, is initially close to the resolution mass of the simulation, $M_{\rm res} \simeq 0.7\ M_\odot$.

We check for rotational support by comparing the specific angular momentum of the SPH particle, $j_{\rm SPH} = v_{\rm rot} d$, with the requirement for centrifugal support, $j_{\rm cent} = \sqrt{G M_{\rm sink} r_{\rm acc}}$, where $v_{\rm rot}$ and d are the rotational velocity and distance of the particle relative to the sink. Once the sink is formed, any SPH particle that satisfies $d < r_{\rm acc}$ and $j_{\rm SPH} < j_{\rm cent}$ is accreted onto the sink. A sink particle can also be merged with another sink particle if these same criteria are met. When the sink is first formed, and after each subsequent accretion event, its position and velocity are set to the mass-weighted average of the particles it has accreted. In this way sink particles can grow and accrete mass over time.

As discussed in Bromm et al. (2002) and Stacy et al. (2010), our criteria for sink formation should be robust. A gas particle must collapse two orders of magnitude above the average density of the surrounding disk, $\simeq 10^{10}$ cm^{-3}, before it is above the density threshold for sink formation. This along with the small value for $r_{\rm acc}$ and the further accretion criterion of non-rotational support ensures that sinks are indeed formed from gravitationally collapsing gas.

Sink particles are held at a constant density of $n_{\rm max} = 10^{12}$ cm^{-3}, a constant temperature of 650 K, and a constant pressure corresponding to its temperature and density. Giving the sink a temperature and pressure prevents the existence of a pressure deficit around the sink that otherwise would yield an artificially high accretion rate (see Bromm et al. 2002; Martel et al. 2006). However, the sink can still evolve in position and velocity due to gravitational and hydrodynamical interactions.

The sink particle method is very useful for various reasons. It eliminates the need to incorporate chemistry, hydrodynamics and radiative transfer at extremely high densities ($n > 10^{12}$ cm^{-3}). More importantly, by stopping the density growth at $n > 10^{12}$ cm^{-3}, the method allows the evolution of the region of interest to be followed for many dynamical times. Without the sink particle method, this would be computationally challenging because the increasing density would lead to prohibitively small numerical timesteps, a problem sometimes called 'Courant myopia'. Finally, the sink particle method allows for a direct measurement of the angular momentum growth and the accretion rate onto the high-density region instead of having to indirectly extrapolate this from the instantaneous density and velocity profiles at the end of the simulation (e.g. Abel et al. 2002; Yoshida et al. 2006).

3 RESULTS

3.1 Sink Growth and Angular Momentum

3.1.1 Accretion Rate

The first minihalo within the cosmological box forms at $z \simeq 20$. The subsequent evolution of the central region of the minihalo to densities of $n = 10^{12}$ cm^{-3} is described in

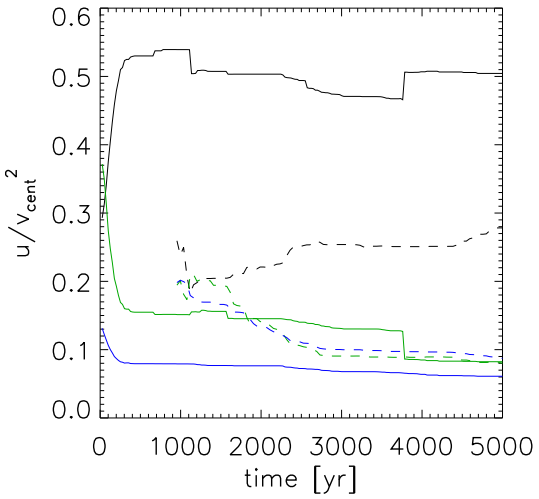

Figure 3. Ratio of the energy of sink-accreted particles to the specific gravitational energy of the sinks ($v_{\rm cent}^2 = GM_{\rm sink}/r_{\rm acc}$). Solid lines are for sink A, and dashed lines are for sink B. Upper (black) lines of each line type represent the energy of rotational motion, middle (green) lines represent the energy of radial motion, and lower (blue) lines represent thermal energy. For both sinks, the rotational energy component dominates for the majority of the accretion time, and a thin Keplerian disk is likely to develop on sub-sink scales.

Stacy et al. (2010). The growth of the first sink that forms, which will be referred to as sink A, is similar to that found in Bromm & Loeb (2004) as well as Stacy et al. (2010). The mass growth is especially similar to that in Stacy et al. (2010) for the first few hundred years, up to several dynamical times after the sink initially forms. Though the sink accretion criteria have some small differences in each of these three studies, this similarity in initial sink growth points especially to the robustness of the density threshold criterion for initial sink formation. After 5000 years of accretion, sink A grows to a mass of 34 $M_\odot$, similar to that found in Bromm & Loeb (2004). However, this is largely due to a significant merger event at around 3800 years, and before this the mass of sink A is around 1/3 below that found in Bromm & Loeb (2004). Furthermore, the final sink mass is slightly less ($\sim$ 20%) than the final mass found in Stacy et al. (2010). The reduced accretion rate found in this current calculation likely arises because a sink is not allowed to accrete a particle if that particle is rotationally supported against infall onto the sink, which is an additional condition that was not included by Stacy et al. (2010). This condition seems to slightly decrease the number of sink merger events, though the growth rate between merger events is also somewhat reduced.

Around 300 years after the formation of sink A, a second sink forms. Meanwhile, as sink A grows, a disk with radius of about 1000 AU develops around the sink, and disk fragmentation allows further sinks to form. By the end of the simulation, 5000 years after sink A first forms, there is a total of four sinks. The sink that is second-most massive, which we will label sink B, has grown almost to 9 $M_\odot$ (Fig. 1), while the remaining two sinks are $\sim$ 1 and 7 $M_\odot$. The overall accretion rate of sink B, $\simeq 2 \times 10^{-3}$ $M_\odot$ yr^{-1}, is around 30% that of sink A, $\simeq 7 \times 10^{-3}$ $M_\odot$ yr^{-1}. The accretion rate for both sinks does not stay at a steady value, however, and actually declines as the sinks grow. To show this we also provide power-law fits to the sink growth (red lines in Fig 1). For sink A, $M_{\rm sink} \propto t^{0.48}$, and $\dot{M} \propto t^{-0.52}$. For sink B, $M_{\rm sink} \propto t^{0.25}$, and $\dot{M} \propto t^{-0.75}$.

3.1.2 Angular Momentum

As the sinks grow in mass, the angular momentum of each particle accreted, $J_{\rm SPH} = m_{\rm SPH} v_{\rm rot} d$, is added to the total angular momentum of the sink, $J_{\rm sink}$. Note that the scale of the sink, $r_{\rm acc} = 50$ AU, is smaller than the radius corresponding to the sonic point:

$$r_{\rm sp} = \frac{GM_*}{c_s^2}, \quad (1)$$

where $c_{\rm s}$ is the sound speed. A typical sink mass is 10 $M_\odot$, and the highest-temperature, high-density ($n > 10^8 {\rm cm}^{-3}$) gas is approximately at 7000 K, or $c_{\rm s} \simeq 7$ km s^{-1}. This yields $r_{\rm sp} \simeq 180$ AU. For the cooler disk gas, $T \sim 500$ K and $c_{\rm s} \simeq 2$ km s^{-1}, so that $r_{\rm sp}$ is larger, ~ 2000 AU, and similar to the size of the large-scale disk. The sinks therefore easily resolve the scale of the sonic point. Angular momentum transport from inside $r_{\rm sp}$ to outside $r_{\rm sp}$ will be difficult once the inflow becomes supersonic (Ulrich 1976; Tan & McKee 2004). In Section 3.2, we will show that the inflow onto the sinks does indeed quickly become supersonic, and in fact the total angular momentum within the sonic point steadily grows as more mass continues to fall in. However, the angular momentum inside $r_{\rm sp}$ can still be redistributed through torques within the large-scale disk.

$J_{\rm sink}$ stays at a fairly steady fraction, $\epsilon = J_{\rm sink}/J_{\rm cent}$, of the angular momentum required for full centrifugal support at the accretion radius, $J_{\rm cent} = M_{\rm sink} j_{\rm cent}$. Figures 1 and 2 show this fraction to range from $\epsilon \simeq 0.45 - 0.5$ for sink A and $\epsilon \simeq 0.25 - 0.35$ for sink B. Thus, on the scale of the accretion radius the sinks never become fully rotationally supported. Rotational velocities of the accreted particles were also recorded, and the total rotational velocity of each

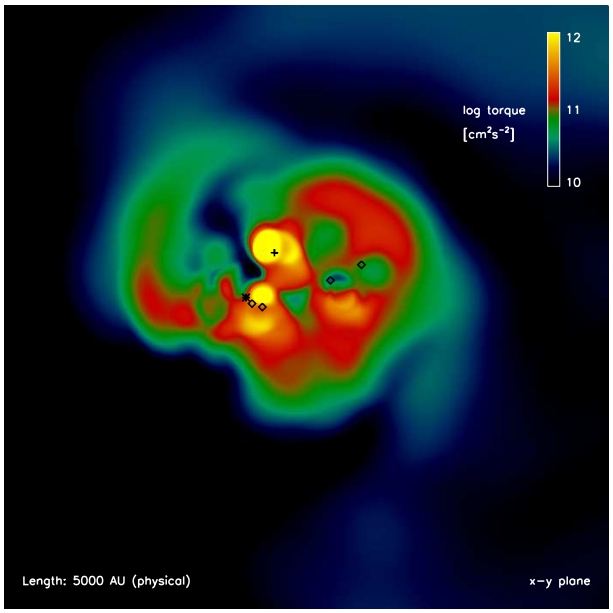

Figure 4. Specific torque acting on the gas within the central 5000 AU of the simulation box, the region enclosing the large-scale star-forming disk. Torques are calculated at a representative time of 2500 years after the first sink forms. Shown is the z-component, perpendicular to disk plane, of all contributions to specific torque as measured from sink A. The asterisk denotes the location of sink A, the cross denotes the location of sink B, and the diamonds are the locations of the remaining lower-mass sinks. There is a total of six sinks, but this number will later be reduced through sink mergers. Note the spiral structure, where gravitational torques will remove angular momentum from the disk center on a timescale of approximately 100-1000 years.

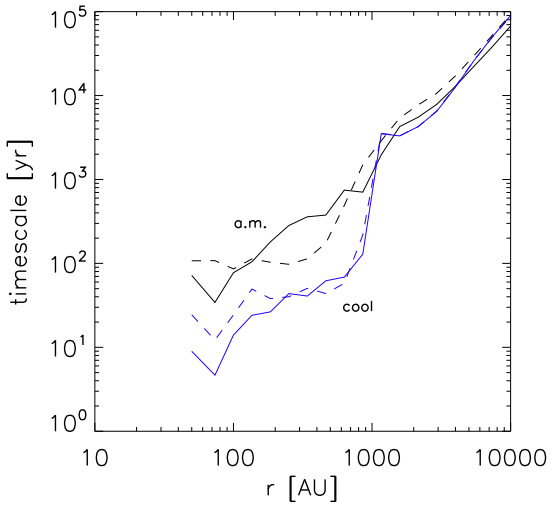

Figure 5. Radially averaged timescales versus distance from the sink at a typical accretion time of 2500 years. The cooling timescale, $t_{\rm cool}$, is shown in blue as the lower set of lines, and the angular momentum loss timescale, $t_{\rm am}$, is shown in black as the upper set of lines. Solid lines are for sink A, and dashed lines are for sink B. For both sinks, $t_{\rm cool}$ is an order of magnitude shorter than $t_{\rm am}$ from the sink edge out to $\sim$ 1000 AU, the edge of the large-scale disk.

sink, $v_{\rm sink}$, can be determined through a mass-weighted average of each accreted particle's $v_{\rm rot}$ (right panel of Fig. 2). Similar to the behavior of $J_{\rm sink}$, $v_{\rm sink}$ stays at the same fairly constant fraction of $v_{\rm cent} = \sqrt{GM_{\rm sink}/r_{\rm acc}}$.

The specific angular momentum of the sinks does not stay perfectly constant, however. Comparing the mild evolution of ϵ with the sinks' mass growth (Fig. 1) shows a general correspondence between them, similar to that found in the simulations of Jappsen & Klessen (2004). For sink B in particular, the shape of the mass versus time curve is very similar to that of the ϵ versus time curve, and the same applies for the first $\sim$ 1000 years of sink A's accretion. These are periods when the mass that flows onto the sinks is gradually increasing in rotational support as the large-scale disk spins up. The gas close to sink A is the first to spin up, and so sink A reaches its maximum ϵ earlier on in the simulation.

It is interesting to compare $J_{\rm sink}$ with the minimum angular momentum required for centrifugal support against infall onto a black hole, as this is one of the minimum requirements for a successful collapsar engine to power a GRB. For a non-rotating black hole of mass $M_{\rm BH}$, the innermost stable circular orbit occurs at $r_{\rm ISCO} = 6GM_{\rm BH}/c^2$. This corresponds to a minimum angular momentum of $J_{\rm ISCO} = \sqrt{6}GM_{\rm BH}^2/c$, which would be slightly smaller for rotating black holes. As can be seen in Fig. 2, sink A and sink B both gather at least an order of magnitude more angular momentum than necessary for a collapsar engine. Whether this large sink-scale angular momentum continues down to stellar scales is discussed below.

3.2 Stellar Rotational Velocity

3.2.1 Thin Accretion Disk

We now address how the measured sink spin can be extrapolated to the scale of the final (MS) Pop III star. To this end, let us compare $J_{\rm sink}$ to angular momentum values corresponding to rotational break-up speeds on stellar scales. A representative value for $J_{\rm break-up}$ can be found assuming a mass of 100 $\rm M_\odot$ and a radius of 5 $\rm R_\odot$, typical for massive Pop III MS stars (e.g. Bromm et al. 2001), though this value may be somewhat larger for high rotation rates. In the latter half of the simulation, $J_{\rm sink}$ for sink B approaches $J_{\rm break-up}$, while sink A easily surpasses $J_{\rm break-up}$ (red line in Fig. 2). If all of sink A's angular momentum became confined to smaller stellar scales this would thus be unphysical. This becomes even more apparent after an analogous examination of sink A's rotational velocity. At the end of the simulation, sink A has a rotational velocity of $v_{\rm sink} = 11$ km s^{-1}. We can extrapolate $v_{\rm sink}$ to the stellar scale of 5 $\rm R_\odot$ by assuming conservation of angular momentum to find $v_* = v_{\rm sink} r_{\rm acc}/5\rm R_\odot$. This turns out to be over 20,000 km s^{-1}, significantly greater than our typical stellar break-up velocity[†], $v_{\rm break-up} \simeq \sqrt{G\,100\rm M_\odot/5R_\odot} \simeq 2000$ km s^{-1} Again, this is unphysical, and serves as an example of the classic angular momentum problem in the context of star formation (e.g. Spitzer 1978; Bodenheimer 1995), now extended to the immediate protostellar environment.

Further insight can be found by evaluating the centrifugal radius,

$$r_{\rm cent} = \frac{j_{\rm sink}^2}{GM_{\rm sink}}, \tag{2}$$

where $j_{\rm sink} = J_{\rm sink}/M_{\rm sink}$. For sink A, in the latter part of the simulation $j_{\rm sink}$ is typically around 8×10^{20} cm^2 s^{-1}, while sink B has $j_{\rm sink} \simeq 3 \times 10^{20}$ cm^2 s^{-1}. At the end of the calculation, $r_{\rm cent} \simeq 10\,$AU for sink A and $r_{\rm cent} \simeq 6\,$AU for sink B, around two orders of magnitude larger than the stellar sizes cited above. At a length sale of $r_{\rm cent}$, contraction would be halted by the centrifugal barrier, and a disk would form. Accretion onto the star would then continue through the disk, and the disk is expected to grow in size. As mentioned above and described in Stacy et al. (2010), in the simulation a disk structure does indeed form and grow well beyond the sink radius. Other very high-resolution simulations also find that primordial gas develops into disks on small scales, less then 50 AU from the star (Clark et al. 2008, 2010).

We therefore infer that much of the angular momentum of the sinks will be distributed in a disk, while most of the sink mass lies within the small $\simeq 5\,\rm R_\odot$ star. There is evidence for the existence of similar disk structure around massive stars in the Galaxy (see, e.g. Cesaroni et al. 2006; Kraus et al. 2010). The nature of the disk can be estimated through a comparison of the thermal energy with the kinetic energy of rotational and radial motion at the sink accretion radius. For gas flow onto a gravitationally dominant central mass, dimensionally the sum of these energies per unit mass, should follow the approximate relation (e.g. Narayan & Yi 1994),

$$v_{\rm rot}^2 + v_{\rm rad}^2 + c_{\rm s}^2 \sim \frac{G\,M_{\rm sink}}{r_{\rm acc}} \equiv v_{\rm cent}^2. \tag{3}$$

Since sink A is the dominant mass, the above relation will more accurately apply to sink A than to sink B, but the energy comparison remains useful for both. Figure 3 shows these energies for each sink relative to its specific gravity, or $v_{\rm cent}^2$, and how these ratios evolve over time. Overall sink ratios were calculated using a mass-weighted average over the individual particles accreted. For sink A, the rotational energy strongly dominates after ~ 300 years and stays dominant for the rest of the simulation. For sink B, the thermal energy and energy of radial motion remain at similarly low values throughout most of the sink's accretion. Around 500 years after sink B forms, the rotational energy becomes the largest contribution to the total sink energy, and this dominance steadily grows for the rest of the calculation. This relatively large amount of rotational energy and low amount of thermal and radial energy for both sinks implies that their sub-sink disks will become thin and Keplerian.

A comparison of the cooling time, $t_{\rm cool}$, with the timescale for angular momentum loss, $t_{\rm am}$, of the gas around the sinks gives further supporting evidence for sub-sink, thin, Keplerian disks. We calculate $t_{\rm am}$ directly from the simulation by recording the acceleration on each gas particle and determining the torque due to numerical viscosity ($\vec{\tau}_{\rm visc}$) as well as the torque exerted by gravity and pressure ($\vec{\tau}_{\rm grav}$ and $\vec{\tau}_{\rm pres}$). The total torque on a given particle within a gas cloud is given by

$$\begin{aligned} \vec{\tau}_{\rm tot} &= \vec{\tau}_{\rm grav} + \vec{\tau}_{\rm pres} + \vec{\tau}_{\rm visc} \\ &= m_{\rm SPH}\vec{d} \times (\vec{a}_{\rm grav} + \vec{a}_{\rm pres} + \vec{a}_{\rm visc}) \ , \end{aligned} \tag{4}$$

where

$$t_{\rm am} \simeq J_{\rm SPH}/|\vec{\tau}_{\rm tot}| \ , \tag{5}$$

and

$$t_{\rm cool} \simeq \frac{nk_{\rm B}T}{\Lambda} \ , \tag{6}$$

with $k_{\rm B}$ being the Boltzmann constant, T the gas temperature, and Λ the cooling rate (in erg cm^{-3} s^{-1}). We find that $\vec{\tau}_{\rm grav}$ and $\vec{\tau}_{\rm pres}$ dominate, accounting for 80% of the total. Figure 4 shows the z-component, perpendicular to the

[†] The formally correct equation for break-up velocity is $v_{\rm break-up} = \sqrt{\frac{2}{3}GM/\rm R}$, where the factor of $\frac{2}{3}$ accounts for deformation due to rotation. However, due to the approximate nature of our calculations, for simplicity we omit this factor of $\frac{2}{3}$ from our calculations.

disk plane, of the specific torque acting upon the gas within the large-scale disk, as measured from the location of sink A. The spiral structure indicates the dominance of gravitational torques which remove angular momentum from the center of the disk on timescales of $100-1000$ years, enabling disk material to be accreted onto the sinks.

Fig. 5 shows these timescales for the gas particles in radially averaged bins. From this we can see that for the gas surrounding each sink, $t_{\rm cool} \sim t_{\rm am}$ at distances greater than 1000 AU. However, at 1000 AU $t_{\rm cool}$ falls below $t_{\rm am}$. This coincides well with the fact that this is the radius of the large-scale disk which embeds the whole stellar multiple system. At the sink edges, $t_{\rm cool}$ is nearly an order of magnitude shorter than $t_{\rm am}$ for both sinks. Thermal energy of the gas is radiated away quickly enough that rotational energy will likely remain dominant. Though torques are active, particularly gravitational ones from the spiral structure in the disk, they are unlikely to remove angular momentum quickly enough to prevent the formation of a sub-sink Keplerian disk once the central stellar mass has grown substantially.

3.2.2 Extrapolation to Stellar Surface

If the entire extent of the sub-sink disks is indeed Keplerian and the disk self-gravity is negligible, then gas within the sinks will rotate at $v(r) \simeq v_{\rm Kep}(r) \simeq \sqrt{GM_*/r}$, where r is the distance from the star, $M_* = f_* M_{\rm sink}$ is the mass of the star, and f_* is the sink mass fraction that ends up in the star while the remaining mass is stored in the disk. For $f_* \lesssim 1$, we will have $v(r) \lesssim \sqrt{GM_{\rm sink}/r}$. If the inner edge of the disk extends all the way to the stellar surface, which is expected if magnetic fields are not important (see §6), then the gas acquired by the star from the accretion disk will be rotating at full Keplerian velocity.

The location of the stellar surface varies as the star's radius evolves. The total angular momentum acquired by the star will depend upon this evolution, and at any given time this total J_* is given by

$$J_*(t) = \int_0^t j(R_*)\dot{M}\,dt = \int_0^t \sqrt{GM_*R_*}\dot{M}\,dt\ , \tag{7}$$

where R_* is the radius of the star. To evaluate this expression, we use the same prescription for the protostellar radial evolution as described in Stacy et al. (2010), which in turn was based upon the earlier work of, e.g. Stahler et al. (1986) and Omukai & Palla (2003). In this prescription, when the protostar first forms as a small hydrostatic core, it will initially undergo a phase of adiabatic accretion and gradual expansion. During this time the protostellar radius will grow as

$$R_{*I} \simeq 50{\rm R}_\odot \left(\frac{M_*}{{\rm M}_\odot}\right)^{1/3} \left(\frac{\dot{M}}{\dot{M}_{\rm fid}}\right)^{1/3}\ , \tag{8}$$

where $\dot{M}_{\rm fid} \simeq 4.4\times10^{-3}{\rm M}_\odot\,{\rm yr}^{-1}$ is a fiducial rate, typical for Pop III accretion. During the subsequent phase of Kelvin-Helmholtz (KH) contraction, the radius will shrink according to

$$R_{*II} \simeq 140{\rm R}_\odot \left(\frac{\dot{M}}{\dot{M}_{\rm fid}}\right) \left(\frac{M_*}{10{\rm M}_\odot}\right)^{-2}\ . \tag{9}$$

We estimate that the transition from adiabatic accretion to KH contraction occurs when the value of R_{*II} falls below that of R_{*I}. For M_* and $\dot{M}$ we employ the power-law fits discussed in §3.1, and we set $M_* \simeq M_{\rm sink}$ in the following analysis. In doing this we have made the simplifying assumption that nearly all of the gas accreted onto the sink quickly flows through the relatively low-mass disk onto the dominating massive star. We also extend the fits to 10^5 years, roughly the point when KH contraction will cease and the star settles onto the MS, with a final radius of $5\,{\rm R}_\odot$. Although the Pop III radial evolution and MS size is based on work that does not account for varying accretion rates and stellar rotation, which may inflate the radius, this should still give a general picture of how the Pop III rotational velocity will evolve.

The resulting evolution of $v_* = J_*/R_*$ for each sink is shown in Fig. 6. Note that during the stars' initial slow expansion, the velocity is not quite at break-up because the stars are gathering mass from gradually increasing radii. Once the stars begin KH contraction, however, the total angular momentum of the stars in fact exceeds break-up, but in this case we assume that the angular momentum will slow the KH contraction accordingly, and we adjust the stellar radius such that the star will again rotate at break-up speed. By setting the right-hand side of Equ. 7 equal to $J_{\rm Kep}$, we find that the radius during this third slowed contraction phase will evolve according to

$$\frac{d}{dt}\ln R_{*III} = -\frac{d}{dt}\ln M \tag{10}$$

Once this phase begins, the star will rotate at break-up speed, $v_* = v_{\rm max} \simeq \sqrt{GM_{\rm sink}/R_*}$.

Given this model, at 10^5 years the star within sink A has mass of 125 $\rm M_\odot$, a radius of 7 $\rm R_\odot$, and a rotational velocity of 1800 km s^{-1}. The star within sink B has mass of 15 $\rm M_\odot$, a radius of 12 $\rm R_\odot$, and a rotational velocity of 500 km s^{-1}. Though details of this model are uncertain, particularly how the accretion rate will evolve during later times beyond the end of our simulation, we can still expect spin-up to occur during KH contraction, likely yielding rotational velocities near break-up speed.

We can also make a more conservative estimate to represent the possible case that sub-sink torques do become strong enough to yield sub-Keplerian rotation rates. Since the overall sink angular momentum stays at a fairly constant fraction of $J_{\rm cent}$, we can apply this to sub-sink scales as well. Then we have $v(r) = \epsilon\, v_{\rm Kep}(r) = \epsilon\sqrt{GM_{\rm sink}/r}$. This is similar to the situation described by Narayan & Yi (1994) in which the gas cannot cool efficiently, causing the accretion flow to stay at approximately the virial temperature. The resulting viscosity is high relative to cold gas, allowing angular momentum to be transported outwards and leading to rotational velocities that remain at a constant fraction $\epsilon < 1$ of $v_{\rm Kep}(r)$ for a large range of radii. At 10^5 years, given $\epsilon = 0.45$ (see Fig. 1), the star within sink A will be rotating at $v_{*,\rm low} \simeq 800$ km s^{-1} (see Fig. 6). This is still a high rotational velocity that is a substantial fraction of the break-up speed. The fastest-rotating stars considered by Woosley & Heger (2006) and Yoon & Langer (2005), for instance, had ϵ values of 0.45 - 0.5. The sink B star would not rotate quite as rapidly due to its lower mass and its slightly lower values of ϵ, but for $\epsilon = 0.35$ the sink B star is still estimated

sink	$M_*(5000\,\mathrm{yr})$ [$\mathrm{M}_\odot$]	$M_*(10^5\,\mathrm{yr})$ [$\mathrm{M}_\odot$]	j_{sink} [$\mathrm{cm^2\ s^{-1}}$]	v_* [$\mathrm{km\ s^{-1}}$]	$v_{*,\mathrm{low}}$ [$\mathrm{km\ s^{-1}}$]
A	34	125	8×10^{20}	1800	800
B	9	15	3×10^{20}	500	300

Table 1. Stellar masses at 5000 years, extrapolated mass at 10^5 years, specific angular momenta of the sinks, final stellar rotational velocities v_*, and the more conservative estimate of stellar rotational velocity $v_{*,\mathrm{low}}$.

to reach a significant rotational velocity of $v_{*,\mathrm{low}} \simeq 300$ km s^{-1}. Also note that, in the conservative case, v_{max} at 10^5 years is slightly higher than that shown in Fig. 6 because KH contraction is no longer slowed by excess angular momentum, and the stars have already reached the MS radius by this time.

4 IMPLICATIONS OF RAPID ROTATION

4.1 Rotational Mixing

Numerous previous studies have found that high rotational velocities such as those predicted from our simulation will alter the stellar evolution (see, e.g. Maeder & Meynet 2000). Models of Maeder (1987), for instance, find that above a critical velocity of 350 km s^{-1} for 20 $\mathrm{M}_\odot$ stars (or 30-40% of break-up velocity), rotationally induced mixing will lead to a very different evolution. Instead of the expected redward track off the MS in the HRD, mixing reduces the chemical gradient throughout the star enough that no extended hydrogen envelope forms. The star smoothly transitions from hydrogen to helium burning, and the stellar radius stays roughly constant while the temperature and luminosity both steadily increase. The star then enters the WR stage, during which heavy mass loss leads to a decrease in the luminosity, though the temperature still remains high. As will be further discussed in the next section, updated studies by Yoon & Langer (2005) and Woosley & Heger (2006) of low-metallicity stars, and also studies by Heger & Langer (2000) of solar-metallicity stars, all similarly find that massive stars with high rotation rates ($\sim$ 40-50% of break-up speed) can undergo chemically homogeneous evolution to become rapidly rotating WR stars.

Rotational mixing is likely to occur according to the calculations we present here, particularly if the stars do indeed rotate at nearly full break-up speed (see Fig. 7). This will have important implications for Pop III feedback. Effective temperatures of stars that undergo such rotational mixing can reach up to an order of magnitude higher than corresponding non-rotating stars, while luminosities may be two to three times as high (see, e.g. Yoon & Langer 2005). This will lead to an increased emission of ionizing radiation at harder wavelengths, so the HII regions will be larger than expected from non-rotating models of stars of the same mass (e.g. Greif et al. 2009).

It is important to note that these results do vary depending upon metallicity and details of the stellar model. For instance, in contrast to earlier studies, Ekström et al. (2008a) find that even rotational speeds of up to 70% of break-up speed will not be sufficient to drive chemically homogeneous evolution. However, they do find rotation to increase the MS lifetime by 10-25%, which again would increase the total amount of ionizing radiation from rotating massive Pop III stars. A final distinction between rotating and non-rotating Pop III evolution is that rotating models generally yield higher total amounts of metals by the end of their nucleosynthesis (Ekström et al. 2008a). Depending on how this metallicity gets spread to the star's surroundings through stellar winds and SN explosions, higher metallicity will enhance the later cooling and collapse of gas when subsequent generations of stars form, most likely lowering their average mass (e.g. Omukai 2000; Bromm et al. 2001; Schneider et al. 2006; Frebel et al. 2007, 2009; Greif et al. 2010)

4.2 GRBs and Hypernovae

The final fate of the stars in our simulation will depend on the mass they reach through accretion, though computational limitations prevent us from following the entire accretion history over the stellar lifetime of ~ 3 Myr. However, extrapolating from the first 5000 years (see Fig. 1) implies that both stars we have discussed are likely to grow significantly more massive. They should certainly be massive enough to avoid a white dwarf fate and make a neutron star or black hole, assuming they do not die as PISNe and leave behind no remnant at all. If they in fact die as core-collapse SNe, we can estimate the effect of rotation on the later SN explosion. Though a black hole remnant is more likely, particularly for the more massive star of sink A, we can derive a more conservative estimate by considering a neutron star remnant. As described in Woosley & Heger (2006), the total rotational energy of a resulting neutron star of radius 12 km and gravitational mass of 1.4 $\mathrm{M}_\odot$ will be $E_{\mathrm{rot}} \simeq 1.1 \times 10^{51}\,(5\,\mathrm{ms}/P)^2$ erg, where P is the rotation period of the neutron star. They find that for E_{rot} to be comparable to the energy of a hypernova, $\sim 10^{52}$ erg, P would need to be ≤ 2 ms. In their low-metallicity models that begin with stars rotating with similar ϵ values to what we found for sink A ($\epsilon \sim 0.45$), they infer resulting neutron star rotation rates that do meet this criterion. They find the same results even for lower ϵ like for those of sink B, though this is only if magnetic torques are not included in the model. Thus, even using the more conservative estimate it is conceivable that the rotational energy reservoir found in sink A and B of our work could be enough to power a hypernova. If the stars rotate more rapidly, at nearly their break-up velocity as we predict, then hypernovae would be even more likely.

Will there still be enough angular momentum for the collapsar engine to work on these stellar scales? If we use the low estimate of $J(r) = \epsilon\, J_{\mathrm{Kep}}(r) = \epsilon \sqrt{G M_{\mathrm{sink}}\, r}$, then on these scales the angular momentum for both sinks still easily meets the required $J > J_{\mathrm{ISCO}}$, especially if their high ϵ values continue as the stars grow to larger masses (see Fig. 7). But will such stars retain this angular momentum

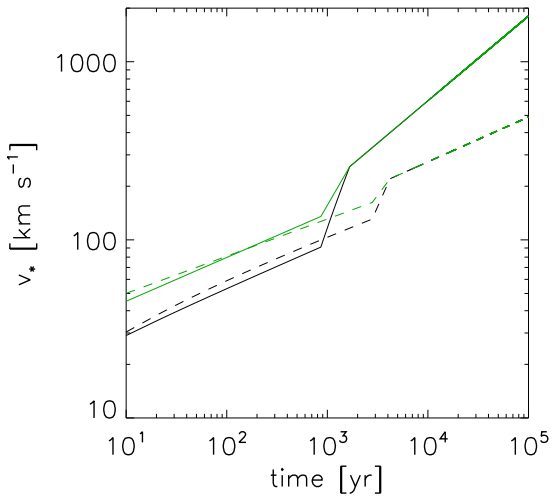

Figure 6. Evolution of stellar rotation. Lower black lines show the rotational velocities v_* of the stars as they initially grow slowly through adiabatic accretion and then undergo KH contraction onto the MS. Upper green lines are the break-up velocities of the stars, $v_{\rm max} \simeq \sqrt{GM_{\rm sink}/R_*}$. Solid lines are for sink A, and dashed lines are for sink B. Note that once KH contraction begins at around 1000 years for sink A and 3000 years for sink B, both stars quickly spin up to the full break-up velocity.

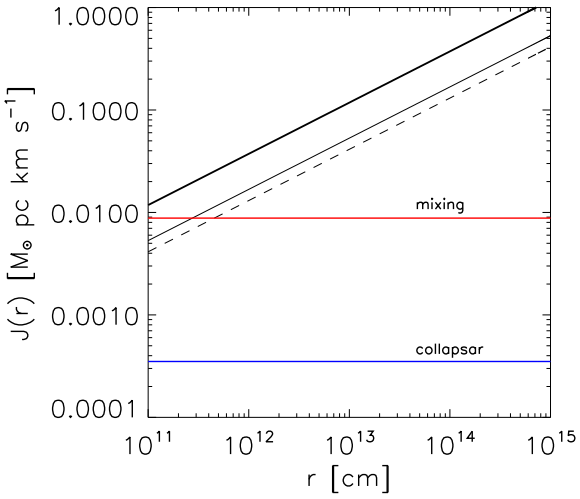

Figure 7. Angular momentum relative to the center of the stars, assuming they have grown to a mass of 100 $M_\odot$ and have an approximate radius of 5 $R_\odot$. Thick black solid line represents the situation of Keplerian rotation where $J(r) = J_{\rm Kep}(r)$. The thin diagonal lines represent the case of $J(r) = \epsilon\, J_{\rm Kep}(r)$. For sink A (solid line), $\epsilon = 0.45$ was used. For sink B (dashed line), we used a smaller value of $\epsilon = 0.35$. Blue line (labeled as "collapsar") shows $J_{\rm ISCO}$. Red line (labeled as "mixing") shows $0.4 * J_{\rm break-up}$, the approximate minimum angular momentum necessary for a low-metallicity star to undergo rotational mixing and chemically homogeneous evolution, as determined by Yoon and Langer (2005) and Woosley and Heger (2006). The angular momentum requirement for the collapsar engine, $J > J_{\rm ISCO}$, is easily met on sub-sink scales. Rotational mixing will readily occur as well as the stars approach their break-up speed.

as they evolve? Low metallicity stellar models in Yoon & Langer (2005) and Woosley & Heger (2006) that were initialized with ϵ values similar to that of sink A show that such stars may indeed be able to retain sufficient amounts of angular momentum in their cores throughout their evolution to the pre-SN stage, depending upon the strength of magnetic fields and the mass loss rate during the WR stage. Though there is still some angular momentum loss in their GRB-forming models, it is limited because rotationally induced mixing allowed these stars to avoid a red giant phase on their path to becoming WR stars. However, Woosley & Heger (2006) generally find that when both magnetic fields and strong mass loss are included in their models, the ability of even their high-ϵ models to meet the GRB requirements becomes borderline.

For the lower ϵ value of 0.35 as found for sink B, a GRB becomes yet less likely, and the star cannot even go through a WR phase unless the models exclude magnetic

fields. However, as discussed in §3.2, the stars within both sink A and sink B are expected to rotate at a much higher fraction of break-up speed - close to 100%. In this case, the above path for becoming a GRB should work yet more readily. Unless there are mechanisms for significant angular momentum transport away from the stars (see §6), the angular momentum condition for the collapsar engine will be met.

5 SUB-SINK FRAGMENTATION

Up to this point we have assumed that each sink will host a single star-disk system, but it is possible that more than one star could exist inside a sink. For instance, a sink merger might lead to a sub-sink binary instead of the presumed coalescence of two stars. We may also consider the possibility that the mass of the sink will fragment and a sub-sink stellar multiple will form in this way. As described by Jappsen & Klessen (2004), this is more likely for higher values of β, the ratio of rotational to gravitational energy. As in Goodman et al. (1993) and Jappsen & Klessen (2004), we can arrive at a simple estimate by assuming that the sinks are undergoing solid-body rotation, have constant angular velocity Ω, and have uniform density. In this case, sink A has $\Omega = 1.5 \times 10^{-9}$ s^{-1} and sink B has $\Omega = 6 \times 10^{-10}$ s^{-1}. We also have

$$\beta = \frac{(1/2)\, I \Omega^2}{qGM^2/R}, \tag{11}$$

where $I = pMR^2$ is the moment of inertia, $p = 2/5$, and $q = 3/5$. In this case sink A has $\beta = 0.070$ and sink B has $\beta = 0.044$, very similar to the values derived for the sinks in Jappsen & Klessen (2004). The requirement for fragmentation ranges from $\beta > 0.01$ to $\beta > 0.1$, depending on the true density structure and thermal properties of gas on sub-sink scales, as well as the effects of magnetic fields (e.g. Boss & Myhill 1995; Boss 1999). For the above values of β, it is thus not entirely certain whether subfragmentation would occur, and this will need to be determined with higher resolution studies.

As discussed earlier, however, disk structure is expected even on sub-sink scales, so it would also be appropriate to examine the Toomre criterion for disk fragmentation:

$$Q = \frac{c_{\rm s} \kappa}{\pi G \Sigma} < 1 \ . \tag{12}$$

Here, Σ is the disk surface density and κ the epicyclic frequency, which is equal to the angular velocity for a disk undergoing Keplerian rotation. However, evaluating Q would require knowledge of disk temperature and surface density on sub-sink scales, which is not available. As discussed in §3.2, cooling is likely to occur faster than angular momentum transport, leading to a sub-sink Keplerian disk. However, gas within these inner regions is more susceptible to heating and other protostellar feedback. This makes disk fragmentation more likely to occur in the cooler outer regions of the disk on scales much larger than the sinks, and indeed such fragmentation is seen in the simulation. Similar points were made in studies such as Kratter & Matzner (2006) and Krumholz et al. (2007).

If a sub-sink binary were to form, however, this could be yet another pathway towards a GRB. As discussed in studies such as Fryer et al. (1999), Bromm & Loeb (2006), and Belczynski et al. (2007), a binary that is tight enough can allow Roche lobe overflow and a common-envelope phase to occur. This will remove the hydrogen envelope of the primary, fulfilling one of the requirements for a collapsar GRB. Even if the stars are rapid rotators, however, Belczynski et al. (2007) find that Pop III binaries will yield GRBs in only a small fraction, $\lesssim 1\%$, of cases. Tidal interactions rarely spin up one of the binary members sufficiently to produce a GRB, and in fact such interactions more often cause the binary members to spin down.

On the other hand, if a wide 50 AU binary were to form within the sinks, this may still leave enough angular momentum for a GRB to form through the rotational mixing pathway. The total angular momentum that will go into the binary orbit will be

$$J_{\rm orb} = M_1 M_2 \frac{\sqrt{aG\,(M_1 + M_2)\,(1 - e^2)}}{M_1 + M_2}, \tag{13}$$

where a is the semimajor axis of the orbit, e is the eccentricity, and M_1 and M_2 are the stellar masses (e.g. Belczynski et al. 2007). If sink A becomes a circular-orbit binary with $M_1 = M_2 = 17$ M$_\odot$, then $J_{\rm orb} = 5 \times 10^{-2}$ M$_\odot$ pc km s^{-1}, about 50% of J$_{\rm sink}$ for sink A at the end of the simulation. If the remaining angular momentum went to the spin of each of the binary components, a GRB may still be able to form.

6 DISCUSSION AND CONCLUSION

We evolved a three-dimensional SPH cosmological simulation until the formation of the first minihalo at $z = 20$, and then followed the evolution of the minihalo gas up to maximum density of 10^{12} cm^{-3}. After this point we used the sink particle method to continue the simulation for 5000 years. A large-scale thick disk of order 1000 AU that formed around the main sink was resolved and so the calculation was able to follow angular momentum transport that occurred within this disk down to resolution length scales of 50 AU. We find that there is sufficient angular momentum in Pop III star-forming cores, represented by the sink particles, to yield rapidly rotating Pop III stars. More specifically, we find that the star-disk systems are likely to rotate at Keplerian speeds. This leads to stellar rotational velocities that can potentially exceed 1000 km s^{-1} for stars with $M \gtrsim 30\,{\rm M}_\odot$. This in turn should lead to chemically homogeneous evolution, yielding hotter and more luminous stars than without rotation. The stars should also retain sufficient spin to power hypernovae as well as collapsar GRBs (e.g. Nomoto et al. 2003; Yoon & Langer 2005; Woosley & Heger 2006). Such GRBs may be observed by the *Swift* satellite, which has already detected GRBs at a redshift as high as $z \approx 8.2$ (Salvaterra et al. 2009; Tanvir et al. 2009), and may also be detected by possible future missions such as JANUS and EXIST.

We emphasize the caveat that we did not fully resolve stellar scales. We have measured the total angular momentum accreted within $r_{\rm acc} \simeq 50$ AU of the star, and we have argued that a Keplerian disk and perhaps a binary is expected to form on sub-sink scales, still leaving enough angular momentum for one or two rapidly rotating stars. However, there are further processes which can transport angular momentum away from rotating stars. For instance, angular momentum may be lost through stellar winds, but the mass and angular momentum loss through winds is expected to

be much lower for low-metallicity and Pop III stars than for higher-metallicity stars (Nugis & Lamers 2000; Kudritzki 2002). Other processes include disk torques induced by gravitational instability as well as viscous torques, which have a variety of sources including hydromagnetic instability (see, e.g. Papaloizou & Lin 1995 for a review).

In particular, the magneto-hydrodynamic (MHD) aspect of Pop III star formation is still very uncertain (e.g. Maki & Susa 2007), and we therefore here neglect any angular momentum loss due to magnetic torques. Earlier work, however, gives some hint as to the possible effect of magnetic fields. Machida et al. (2008) conclude that if a star-forming primordial cloud has a large enough initial magnetic field ($B > 10^{-9} \left[n/10^3 \mathrm{cm}^{-3}\right]^{2/3}$ G), a protostellar jet will be driven provided that the cloud's rotational energy is less than its magnetic energy. However, Xu et al. (2008) find that the Biermann battery mechanism and flux freezing alone will not amplify magnetic fields in a collapsing halo quickly enough to reach this threshold value. In contrast, small-scale dynamo amplification as described by Schleicher et al. (2010) could generate sufficient magnetic fields for the magneto-rotational instability (MRI) to operate in primordial protostellar disks (e.g. Balbus & Hawley 1991). The resulting turbulent viscosity would facilitate outward angular momentum transfer in the disk, and it may further allow generation of sufficient magnetic field strength to drive collimated protostellar outflows that can also remove angular momentum (e.g. Tan & Blackman 2004; Silk & Langer 2006). This may furthermore facilitate some form of 'disk-locking' as described by various authors such as Koenigl (1991), Shu et al. (1994), and Matt & Pudritz (2005), where the stellar rotation will be 'locked' to a rate given by the star's mass, accretion rate, magnetic field strength, and radius. Such a model was described by Koenigl (1991), for example, to yield $\Omega_* \sim G M_*^{5/7} \dot{M}^{3/7} B^{-6/7} R_*^{-18/7}$, where Ω_* is the star's angular velocity and B the stellar magnetic field strength. In short, the rate at which these effects will remove angular momentum from the star is very dependent on the still uncertain magnetic field strength in Pop III star forming regions, although such effects are a likely part of the explanation for slowly rotating stars observed in the Galaxy (see, e.g. Bodenheimer 1995). Whether this also applies in the early Universe will be best determined through future numerical simulations. A three-dimensional cosmological simulation that can resolve stellar scales and follow MHD processes for many dynamical times is highly computationally demanding. For the moment, our preliminary calculation provides an upper limit for the Pop III stellar rotation rate.

A comparison with Jappsen & Klessen (2004) shows interestingly similar results. The average specific angular momentum of their protostellar objects was 8×10^{19} cm^2 s^{-1}, and the typical mass of each object was $\simeq 1$ M$_\odot$. They find that the specific angular momentum increases with mass, with $j \propto M^{2/3}$ being their preferred fit. Our sink particles are 9 and 34 times more massive and so should have specific angular momenta about 4 and 10 times higher, or $3 - 8 \times 10^{20}$ cm^2 s^{-1}. This is indeed the specific angular momentum measured for our sinks. This also compares well with the range of observed angular momenta of various structures in the Milky Way. For instance, the average specific angular momentum of binaries in the Taurus star-forming region was found by Simon et al. (1995) to be $j \simeq 2 \times 10^{20}$ cm^2 s^{-1}, and similar values were found for G-dwarf stars by Duquennoy & Mayor (1991). For less-evolved structures, Caselli et al. (2002) found an average of $j = 7 \times 10^{20}$ cm^2 s^{-1} for cores of mean mass of 6 M$_\odot$. Goodman et al. (1993) observed larger cores of approximately 50 M$_\odot$ and obtained an average of $j \simeq 2 \times 10^{21}$ cm^2 s^{-1}. These cores would be expected to lose angular momentum as they evolve into protostars, leading to smaller values similar to those observed in stellar binaries. Despite the different initial conditions which give rise to Pop III stars versus stars in our Galaxy, the overall angular momentum reservoir for both is very similar. Thus, just as rapidly rotating massive stars are observed today (e.g. Huang & Gies 2008; Wolff et al. 2008), rapidly rotating massive stars seem likely to exist in the early Universe as well. Unless they are spun down by processes such as magnetic torques or bipolar outflows, such rapid rotation rates must play an important role in the evolution and final state of the first stars.

ACKNOWLEDGMENTS

AS thanks Andreas Pawlik and Milos Milosavljevic for helpful discussions. The authors also thank Sylvia Ekström for valuable feedback. This work was supported in part by NSF grants AST-0708795 and AST1009928 and NASA ATFP grant NNX08AL43G (for VB), and NSF grant AST-0907890 and NASA grants NNX08AL43G and NNA09DB30A (for AL). The simulations presented here were carried out at the Texas Advanced Computing Center (TACC).

References

Abel T., Bryan G. L., Norman M. L., 2002, Sci, 295, 93
Alvarez M. A., Bromm V., Shapiro P. R., 2006, ApJ, 639, 621
Balbus S. A., Hawley J. F., 1991, ApJ, 376, 214
Barkana R., Loeb A., 2001, Phys. Rep., 349, 125
Bate M. R., Bonnell I. A., Price N. M., 1995, MNRAS, 277, 362
Bate M. R., Burkert A., 1997, MNRAS, 288, 1060
Belczynski K., Bulik T., Heger A., Fryer C., 2007, ApJ, 664, 986
Bodenheimer P., 1995, ARA&A, 33, 199
Boss A. P., 1999, ApJ, 520, 744
Boss A. P., Myhill E. A., 1995, ApJ, 451, 218
Bromm V., Coppi P. S., Larson R. B., 2002, ApJ, 564, 23
Bromm V., Ferrara A., Coppi P. S., Larson R. B., 2001, MNRAS, 328, 969
Bromm V., Kudritzki R. P., Loeb A., 2001, ApJ, 552, 464
Bromm V., Larson R. B., 2004, ARA&A, 42, 79
Bromm V., Loeb A., 2002, ApJ, 575, 111
Bromm V., Loeb A., 2004, New Astron., 9, 353
Bromm V., Loeb A., 2006, ApJ, 642, 382
Bromm V., Yoshida N., Hernquist L., 2003, ApJ, 596, L135
Bromm V., Yoshida N., Hernquist L., McKee C. F., 2009, Nat, 459, 49
Caselli P., Benson P. J., Myers P. C., Tafalla M., 2002, ApJ, 572, 238

Cesaroni R., Galli D., Lodato G., Walmsley M., Zhang Q., 2006, Nature, 444, 703
Ciardi B., Ferrara A., 2005, SSR, 116, 625
Clark P. C., Glover S. C. O., Klessen R. S., 2008, ApJ, 672, 757
Clark P. C., Glover S. C. O., Klessen R. S., Bromm V., 2010, ApJ, submitted (arXiv: 1006.1508)
Duquennoy A., Mayor M., 1991, A&A, 248, 485
Ekström S., Meynet G., Chiappini C., Hirschi R., Maeder A., 2008a, A&A, 489, 685
Ekström S., Meynet G., Maeder A., Barblan F., 2008b, A&A, 478, 467
Frebel A., Johnson J. L., Bromm V., 2007, MNRAS, 380, L40
Frebel A., Johnson J. L., Bromm V., 2009, MNRAS, 392, L50
Fryer C. L., Woosley S. E., Hartmann D. H., 1999, ApJ, 526, 152
Glover S., 2005, Space Sci. Rev., 117, 445
Goodman A. A., Benson P. J., Fuller G. A., Myers P. C., 1993, ApJ, 406, 528
Gou L. J., Mészáros P., Abel T., Zhang B., 2004, ApJ, 604, 508
Greif T. H., Glover S. C. O., Bromm V., Klessen R. S., 2010, ApJ, 716, 510
Greif T. H., Johnson J. L., Bromm V., Klessen R. S., 2007, ApJ, 670, 1
Greif T. H., Johnson J. L., Klessen R. S., Bromm V., 2009, MNRAS, 399, 639
Haiman Z., Thoul A. A., Loeb A., 1996, ApJ, 464, 523
Heger A., Langer N., 2000, ApJ, 544, 1016
Heger A., Woosley S. E., 2002, ApJ, 567, 532
Heger A., Woosley S. E., Spruit H. C., 2005, ApJ, 626, 350
Huang W., Gies D. R., 2008, ApJ, 683, 1045
Izzard R. G., Ramirez-Ruiz E., Tout C. A., 2004, MNRaS, 348, 1215
Jappsen A., Klessen R. S., 2004, A&A, 423, 1
Johnson J. L., Greif T. H., Bromm V., 2007, ApJ, 665, 85
Kitayama T., Yoshida N., Susa H., Umemura M., 2004, ApJ, 613, 631
Koenigl A., 1991, ApJ, 370, L39
Kratter K. M., Matzner C. D., 2006, MNRAS, 373, 1563
Kraus S., Hofmann K., Menten K. M., Schertl D., Weigelt G., Wyrowski F., Meilland A., Perraut K., Petrov R., Robbe-Dubois S., Schilke P., Testi L., 2010, Nat, 466, 339
Krumholz M. R., Klein R. I., McKee C. F., 2007, ApJ, 656, 959
Kudritzki R. P., 2002, ApJ, 577, 389
Lee C., Brown G. E., Wijers R. A. M. J., 2002, ApJ, 575, 996
Lee W. H., Ramirez-Ruiz E., 2006, ApJ, 641, 961
Loeb A., 2010, How Did the First Stars and Galaxies Form? Princeton University Press, Princeton
Machida M. N., Matsumoto T., Inutsuka S., 2008, ApJ, 685, 690
Madau P., Ferrara A., Rees M. J., 2001, ApJ, 555, 92
Maeder A., 1987, A&A, 178, 159
Maeder A., Meynet G., 2000, ARA&A, 38, 143
Maki H., Susa H., 2007, PASJ, 59, 787
Martel H., Evans N. J., Shapiro P. R., 2006, ApJS, 163, 122
Matt S., Pudritz R. E., 2005, ApJ, 632, L135
Mori M., Ferrara A., Madau P., 2002, ApJ, 571, 40
Naoz S., Bromberg O., 2007, MNRAS, 380, 757
Narayan R., Yi I., 1994, ApJ, 428, L13
Nomoto K., Maeda K., Umeda H., Ohkubo T., Deng J., Mazzali P., 2003, Prog. Theor. Phys. Suppl., 151, 44
Norman M. L., O'Shea B. W., Paschos P., 2004, ApJ, 601, L115
Nugis T., Lamers H. J. G. L. M., 2000, A&A, 360, 227
Omukai K., 2000, ApJ, 534, 809
Omukai K., Palla F., 2003, ApJ, 589, 677
Papaloizou J. C. B., Lin D. N. C., 1995, ARA&A, 33, 505
Petrovic J., Langer N., Yoon S., Heger A., 2005, A&A, 435, 247
Salvaterra R., Della Valle M., Campana S., Chincarini G., Covino S., D'Avanzo P., Fernández-Soto A., Guidorzi C. e. a., 2009, Nat, 461, 1258
Schleicher D. R. G., Banerjee R., Sur S., Arshakian T. G., Klessen R. S., Beck R., Spaans M., 2010, A&A, accepted (arXiv: 1003.1135)
Schneider R., Omukai K., Inoue A. K., Ferrara A., 2006, MNRAS, 369, 1437
Shu F., Najita J., Ostriker E., Wilkin F., Ruden S., Lizano S., 1994, ApJ, 429, 781
Silk J., Langer M., 2006, MNRAS, 371, 444
Simon M., Ghez A. M., Leinert C., Cassar L., Chen W. P., Howell R. R., Jameson R. F., Matthews K., Neugebauer G., Richichi A., 1995, ApJ, 443, 625
Sokasian A., Yoshida N., Abel T., Hernquist L., Springel V., 2004, MNRAS, 350, 47
Spitzer L., 1978, Physical Processes in the Interstellar Medium. Wiley, New York
Springel V., Hernquist L., 2002, MNRAS, 333, 649
Springel V., Yoshida N., White S. D. M., 2001, New Astron., 6, 79
Spruit H. C., 2002, A&A, 381, 923
Stacy A., Greif T. H., Bromm V., 2010, MNRAS, 403, 45
Stahler S. W., Palla F., Salpeter E. E., 1986, ApJ, 302, 590
Suwa Y., Ioka K., 2010, arXiv:1009.6001
Tan J. C., Blackman E. G., 2004, ApJ, 603, 401
Tan J. C., McKee C. F., 2004, ApJ, 603, 383
Tanvir N. R., Fox D. B., Levan A. J., Berger E., Wiersema K., Fynbo J. P. U., Cucchiara A., Krühler T., Gehrels N., Bloom J. S., Greiner J. e. a., 2009, Nat, 461, 1254
Tegmark M., Silk J., Rees M. J., Blanchard A., Abel T., Palla F., 1997, ApJ, 474, 1
Tornatore L., Ferrara A., Schneider R., 2007, MNRAS, 382, 945
Turk M. J., Abel T., O'Shea B., 2009, Sci, 325, 601
Ulrich R. K., 1976, ApJ, 210, 377
Wada K., Venkatesan A., 2003, ApJ, 591, 38
Whalen D., Abel T., Norman M. L., 2004, ApJ, 610, 14
Wise J. H., Abel T., 2008, ApJ, 685, 40
Wolff S. C., Strom S. E., Cunha K., Daflon S., Olsen K., Dror D., 2008, AJ, 136, 1049
Woosley S. E., 1993, ApJ, 405, 273
Woosley S. E., Bloom J. S., 2006, ARA&A, 44, 507
Woosley S. E., Heger A., 2006, ApJ, 637, 914
Xu H., O'Shea B. W., Collins D. C., Norman M. L., Li H., Li S., 2008, ApJ, 688, L57
Yoon S., Langer N., 2005, A&A, 443, 643
Yoshida N., Abel T., Hernquist L., Sugiyama N., 2003, ApJ, 592, 645

Yoshida N., Omukai K., Hernquist L., Abel T., 2006, ApJ, 652, 6
Zhang W., Woosley S. E., Heger A., 2004, ApJ, 608, 365